Electronic Supplementary Information

Thermally reduced graphene oxide membrane interlayered with in situ synthesized nanospacer for water desalination

*Hongyu Ma,[a] Xiaofang Chen,[a] Shabin Mohammed,[a] Yaoxin Hu,[a] Jun Lu,[a] George P. Simon,[b] Hongjuan Hou [c] and Huanting Wang [a]**

[a] *Department of Chemical Engineering, Monash University, Clayton, Victoria 3800, Australia.*

[b] *Department of Materials Science and Engineering, Monash University, Clayton, Victoria 3800, Australia.*

[c] *Energy and Environment Research Institute, Baosteel Group Corporation, Shanghai 201900, China.*

Corresponding author: *Huanting Wang Huanting.Wang@monash.edu

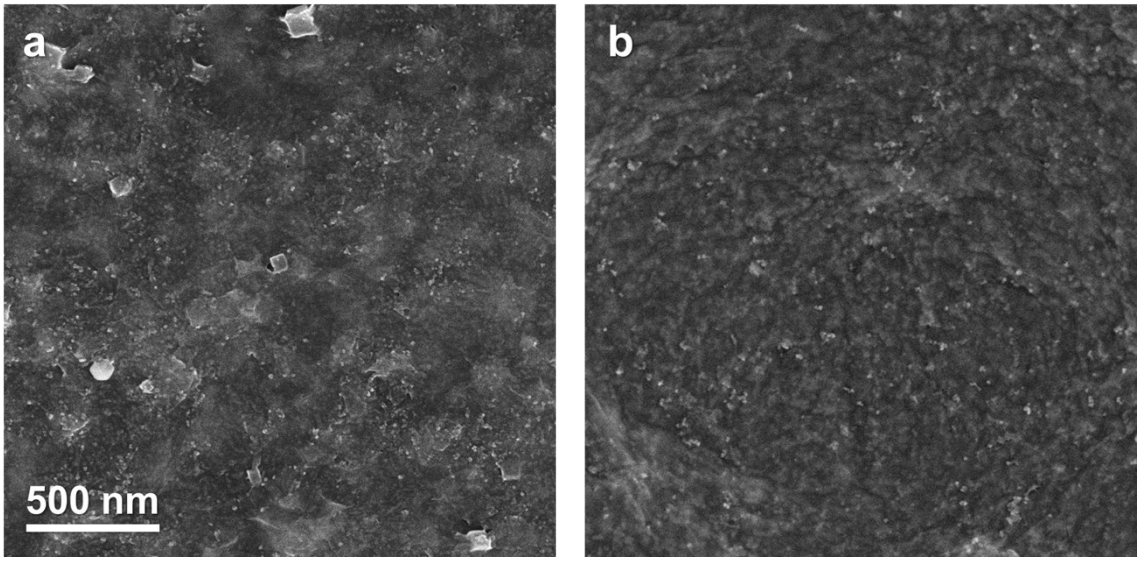

Figure S1. Comparison of the *in situ* synthesized Prussian blue (PB) particles with different reactants. (a) SEM image of graphene oxide (GO) and PB composite synthesized from the direct coordination of Fe^{2+} and $[Fe(CN)]^{3-}$ ions. (b) SEM image of GO/PB composite synthesized from Fe^{3+} and $[Fe(CN)]^{3-}$ ions. The scales for the two images are the same.

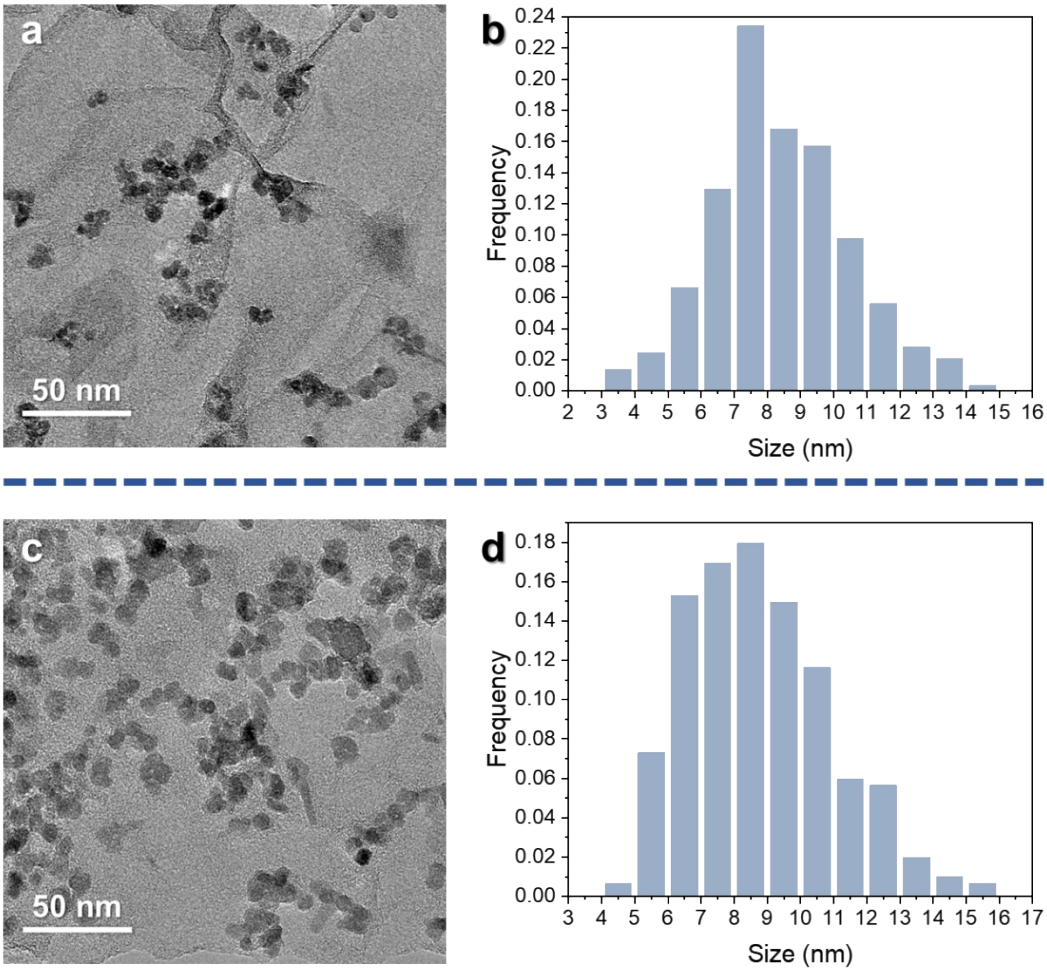

Figure S2. Comparison of the *in situ* synthesized PB particles before and after thermal reduction. (a) Transmission electron microscope (TEM) image of the GO/PB composite. (b) Size distribution of the PB particles before reduction. (c) TEM image of thermally reduced GO and PB (rGO/PB) composite. (d) Size distribution of PB particles after thermal treatment.

Note: The size distribution was based on over 200 measurements of the particles. The particle distribution density for rGO/PB appears higher than GO/PB due to the agglomeration and stacking of the rGO/PB nanosheets. After the thermal reduction, most of the hydroxide functional groups on rGO nanosheets were removed, which resulted in less dispersity in ethanol during TEM sample preparation.

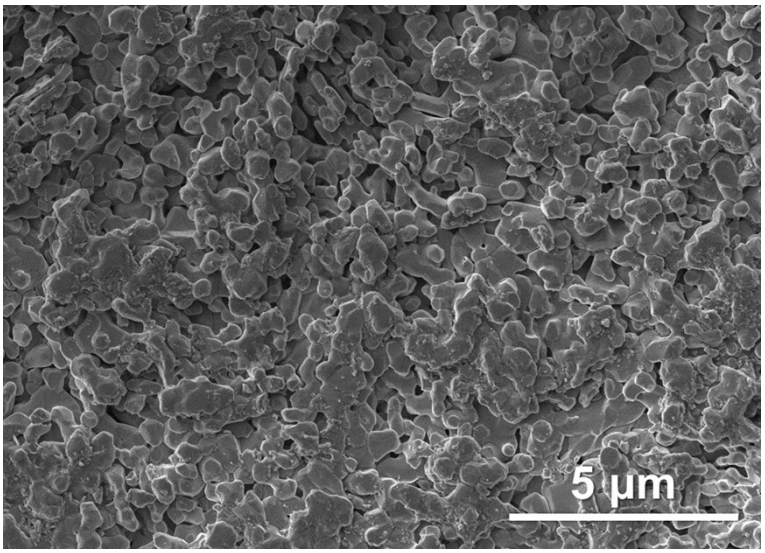

Figure S3. Scanning electron microscope (SEM) image of the homemade Al_2O_3 substrate.

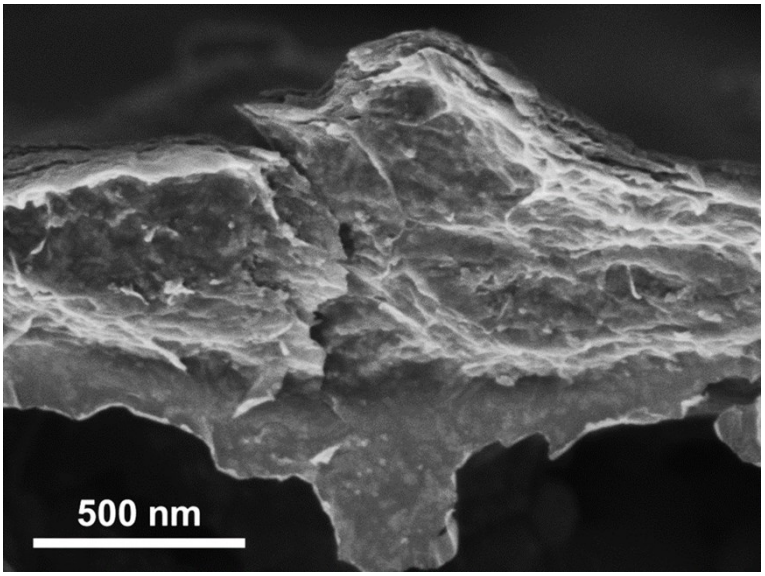

Figure S4. SEM image of a peeled off cross-section area of the rGO/PB membrane. Nanoparticles are intercalated uniformly in the interior part of the membrane. The curvature of the surface also indicates the channels supported by the particles.

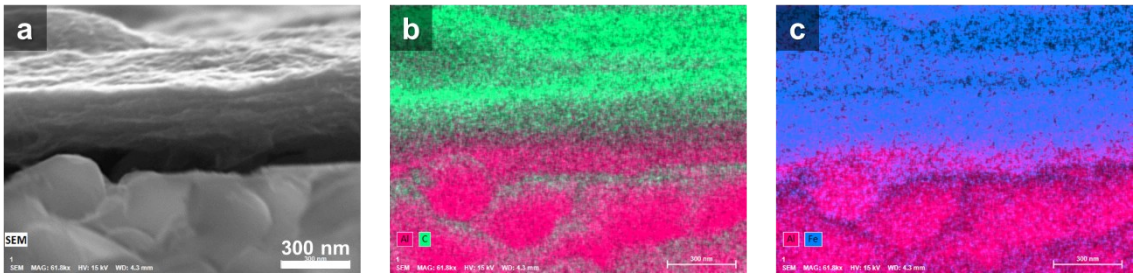

Figure S5. Energy Dispersive X-ray (EDX) analysis of the rGO/PB membrane cross-section. (a) The corresponding SEM image of the membrane cross-section. (b) EDX mapping of Al (Red) and C (Green) elements. (c) EDX mapping of Al (Red) and Fe (Blue) elements. The scales for all images are the same.

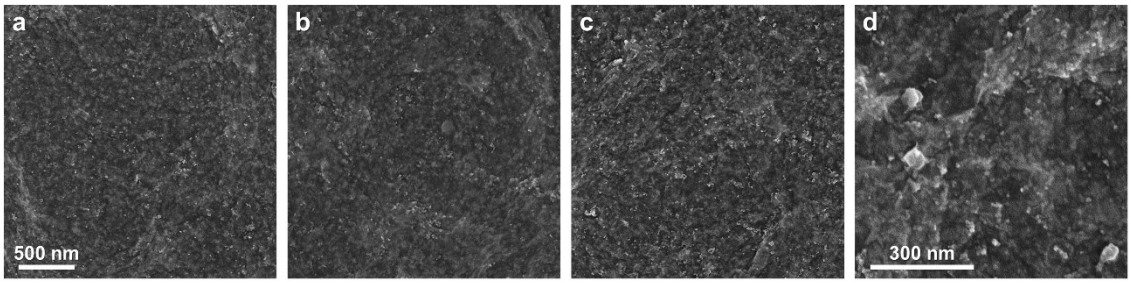

Figure S6. SEM images of rGO/PB composite membrane of 10:4 (a), 10:6 (b), 10:8 (c), and 10:10 (d). The scales for (a), (b), and (c) images are the same.

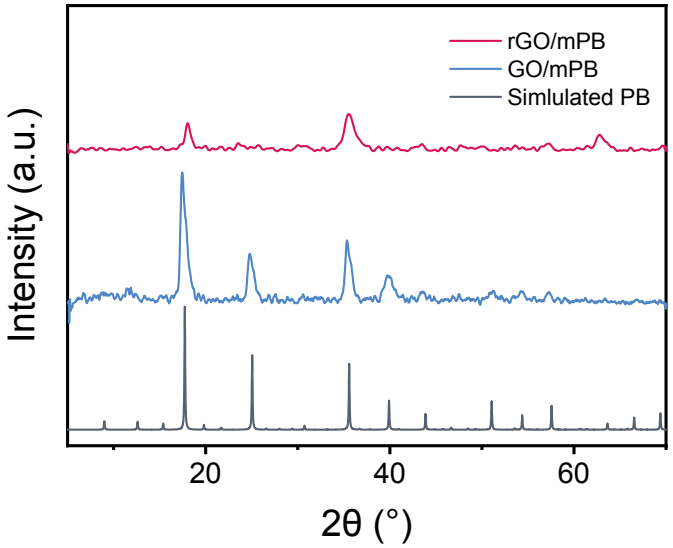

Figure S7. XRD results of the graphene oxide grown with the excess amount of PB

particles before and after thermal reduction. The large amount of PB on GO (GO/mPB) generated typical Prussian blue XRD patterns. After the thermal reduction, the rGO/mPB sample showed peaks at 17.9°, 35.6° and 62.8°, which could be the characteristic (111), (311) and (440) peaks of Fe_3O_4 respectively.[1] This indicated that PB particles decomposed and were possibly oxidized by the generated oxygen from the GO during the thermal reduction.[2]

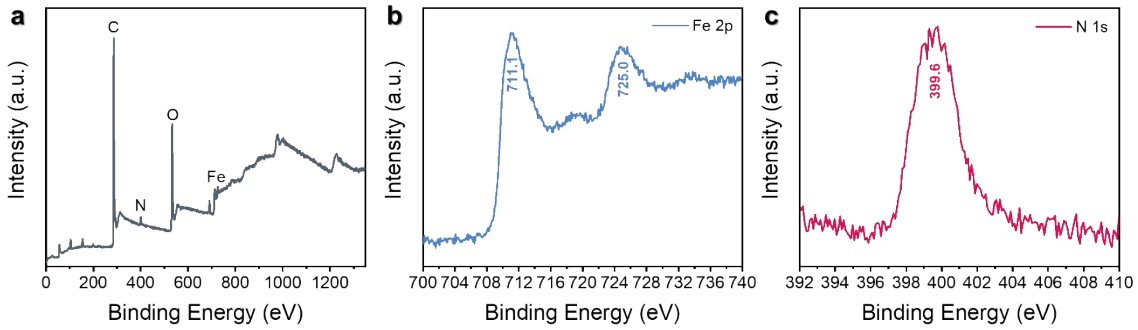

Figure S8. X-ray photoelectron spectroscopy (XPS) analysis of the rGO/PB membrane with wide scan spectrum (a), Fe 2p spectrum (b), and N 1s spectrum (c). The Fe 2p spectrum showed the characteristic peaks of $Fe2p_{3/2}$ and $Fe2p_{1/2}$ at 711.1 eV and 725.0 eV respectively, which could originate from Fe_3O_4 particles.[3] The main peak at 399.6 eV in the N 1s spectrum indicated the binding energy of C-NH_2,[4] which could be generated from the reaction between GO and the decomposed PB particles during the thermal treatment.[5]

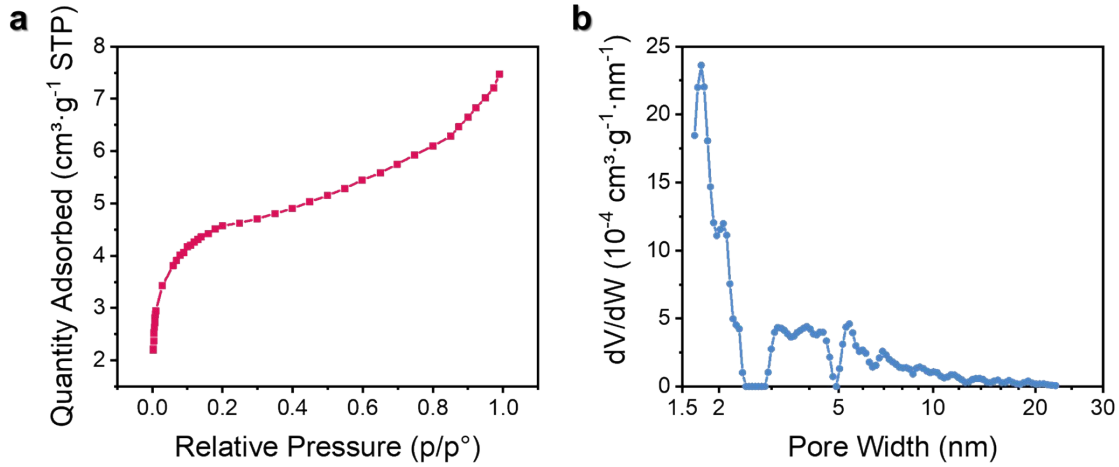

Figure S9. Argon adsorption results of the rGO/PB membranes. (a) Adsorption isotherm. (b) Calculated pore size distribution (PSD).

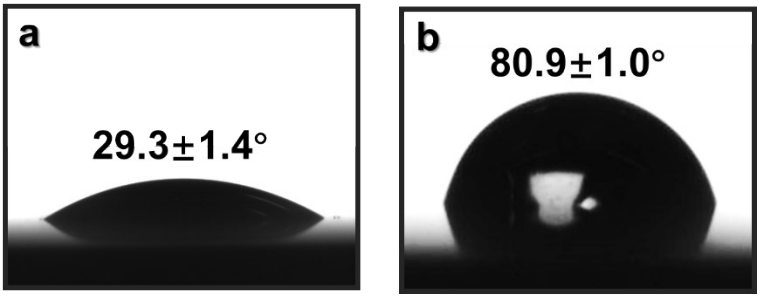

Figure S10. Water contact angle measurement of the unmodified GO membrane (a), and rGO membrane (b).

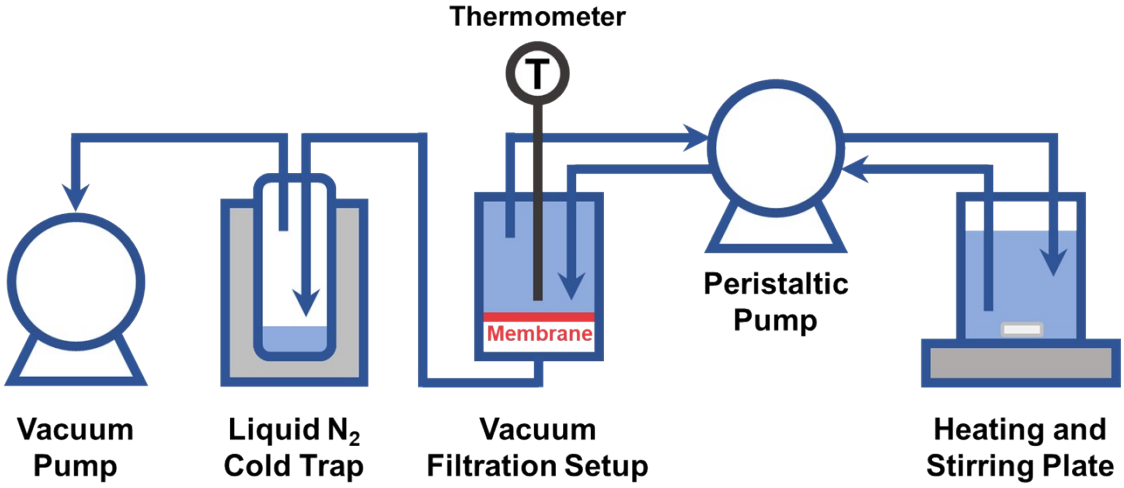

Figure S11. Schematic illustration of desalination performance testing setup.

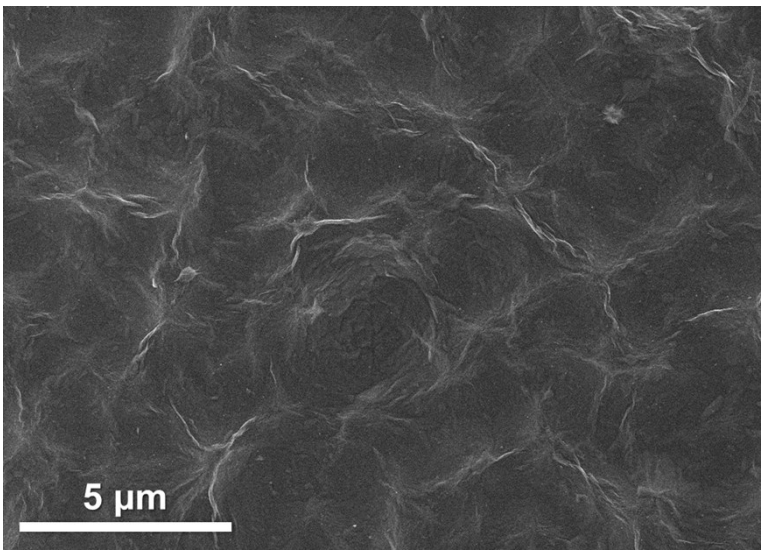

Figure S12. SEM image of the thermally reduced GO membrane.

Scheme S1:

Liquid Entry Pressure (LEP) measurement: The rGO/PB membrane was mounted on a dead-end cell, where the DI water was used as the feed and pressurized by N_2 gas cylinder. The applied pressure was read from the gas valve of the cylinder, and for a determined pressure value, the membrane was continuously tested for 8 hours. When we applied the pressure up to 675 kPa (0.675bar), there was no liquid water permeation in the 8 hours' testing for 3 individual membranes. And when the applied pressure has increased to 700 kPa (0.7 bar), water came out at the permeate side. However, after we dismounted the membrane, we found that there were cracks on our Al_2O_3 substrates. The porous structure of the Al_2O_3 substrates could be the reason that it did not have enough mechanical strength to stand the high pressure. According to these results, we concluded that the LEP of rGO/PB membrane was enough to prevent the liquid solution from entering during the vacuum-asissted desalination, which had the pressure difference of ~0.9 bar in the operation.

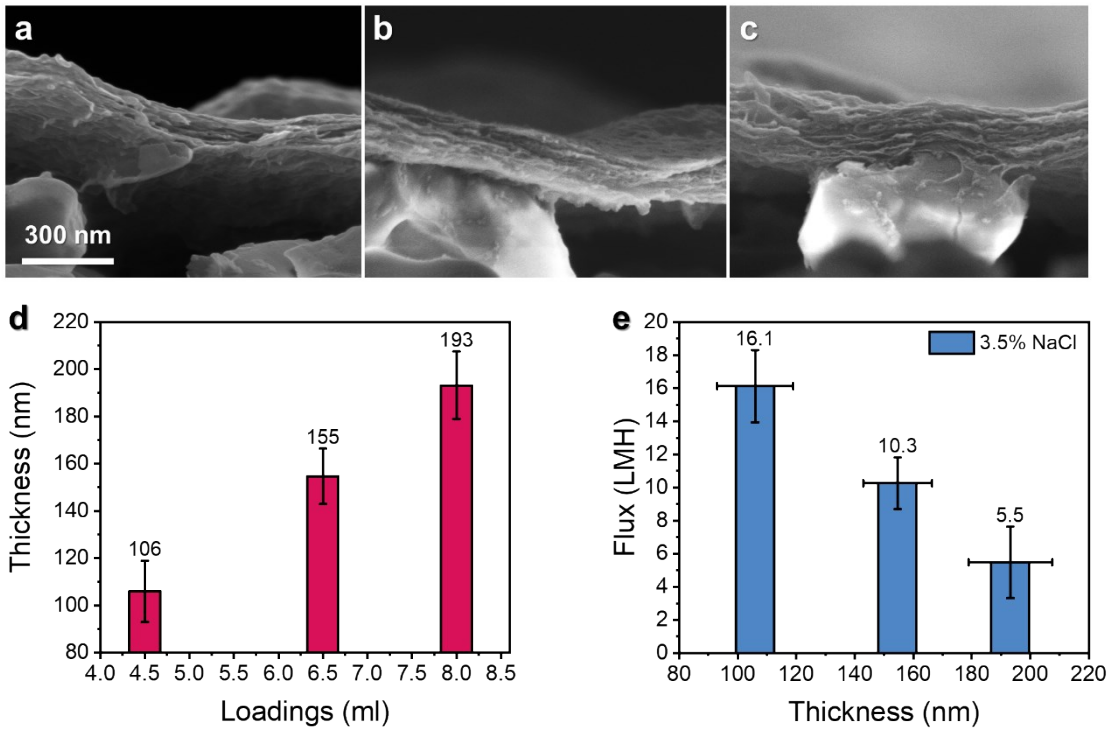

Figure S13. Membrane 10:8 with different thickness by changing the loadings, and its influence on the performance. SEM images of the membrane cross-section with the loadings of 4.5 ml (a), 6.5 ml (b), and 8.0 ml (c). The scales of all the SEM images are the same. (d) Membrane thickness with increasing loadings. (e) Flux results of 3.5 wt% NaCl solution at room temperature from membranes of different thicknesses.

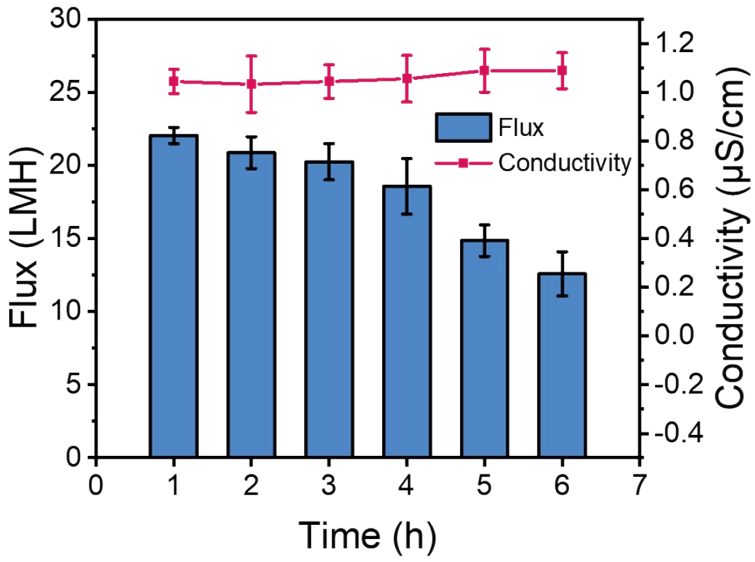

Figure S14. The direct contact membrane distillation (DCMD) performance of the membrane 10:8, and the conductivity of the permeate side solution. The heated feed solution (200mL 3.5% NaCl solution at 60 °C) and permeate side solution (200mL Mili-Q water) were circulated on the two sides of the rGO/PB membrane. The permeate solution container was placed on an electronic balance, and the flux was calculated based on the mass change. The mass change and the conductivity of the permeate side solution were measured hourly, and the DMCD process was carried out for 6 hours.

Table S1. The evaporation-changed based desalination performance from the literature.

Main compositions of the membrane	Desalination type	Feed solution concentration	Feed temperature (°C)	Flux (LMH)	Reference
Teflon coating/Silica/PVDF	VMD	3.5% NaCl with SDS	70	24.9	*Environ. Sci. Technol.* **2018**,[6]
PVDF	VMD	9% NaCl	30	~15	*J. Memb. Sci.* **2020**,[7]

PVDF	VMD	9% NaCl	50	~50	*J. Memb. Sci.* **2020**,[7]
PVDF	VMD	9% NaCl	70	~100	*J. Memb. Sci.* **2020**,[7]
Porous Carbon	VMD	3% NaCl	20	~16	*Nat. Nanotechnol.* **2018**,[8]
Porous Carbon	VMD	3% NaCl	40	~62	*Nat. Nanotechnol.* **2018**,[8]
Porous Carbon	VMD	3% NaCl	50	~91	*Nat. Nanotechnol.* **2018**,[8]
Porous Carbon	VMD	3% NaCl	60	~122	*Nat. Nanotechnol.* **2018**,[8]
Porous Carbon	VMD	3% NaCl	70	~164	*Nat. Nanotechnol.* **2018**,[8]
Porous Carbon	VMD	3% NaCl	80	~203	*Nat. Nanotechnol.* **2018**,[8]
MXene	PV	3.5% NaCl	65	95.4	*J. Memb. Sci.* **2018**,[9]
PAMAM/GO	PV	3.5% NaCl	30	31	*J. Mater. Chem. A* **2019**,[10]
PAMAM/GO	PV	3.5% NaCl	70	124	*J. Mater. Chem. A* **2019**,[10]
PVA/PAN	PV	3.5% NaCl	35	~47	*Nat. Commun.* **2020,**[11]
PVA/PAN	PV	3.5% NaCl	45	~80	*Nat. Commun.* **2020,**[11]
PVA/PAN	PV	3.5% NaCl	55	~123	*Nat. Commun.* **2020,**[11]
PVA/PAN	PV	3.5% NaCl	65	~162	*Nat. Commun.* **2020,**[11]
PVA/PAN	PV	3.5% NaCl	75	~212	*Nat. Commun.* **2020,**[11]

Note: The flux values which were approximately obtained from the reported figures were marked with '~' before the values.

Table S2. The desalination performance comparison of the nanomaterials intercalated reduced GO membranes from the literature.

Main compositions of the membrane	Desalination type	Feed solution	Applied pressure	Flux	Rejection (%)	Reference
TiO_2 nanoparticle/rGO	Nanofiltration	5 mM NaCl	1 bar	~75 LMH/bar	~40	*J. Mater. Chem. A* **2019**,[12]
TiO_2 nanorod/rGO	Nanofiltration	2 mM NaCl	90 kPa	32.9 LMH/bar	41.2	*Chem. Phys. Lett.* **2020,**[13]
TiO_2 nanorod/rGO	Nanofiltration	2 mM NaCl	90 kPa	52.1 LMH/bar	35.6	*Chem. Phys. Lett.* **2020,**[13]
Ag nanoparticle /PDA-rGO	Nanofiltration	2000 ppm NaCl	3-4 bar	6.11 LMH/bar	65.6	*Desalination* **2018,**[14]
UiO-66-$(COOH)_2$ nanoparticle/prGO	Nanofiltration	10mM Na_2SO_4	1 bar	~22 LMH/bar	32.6	*Chemosphere* **2018,**[15]
Cu nanoparticle /PFA-rGO	Nanofiltration	0.1% NaCl	4 bar	~23 LMH/bar	~10	*ACS Appl. Mater. Interfaces* **2017,**[16]
Carbon nanotube /rGO	Nanofiltration	0.01M NaCl	5 bar	8.02 LMH/bar	51.4	*ACS Appl. Mater. Interfaces* **2015,**[17]
Carbon nanotube /rGO	Nanofiltration	0.01M NaCl	5 bar	12.1 LMH/bar	39.6	*ACS Appl. Mater. Interfaces* **2015,**[17]
PSS-Halloysite nanotubes/rGO	Nanofiltration	1000 ppm NaCl	400 kPa	4.96 LMH/bar	16.8	*Desalination* **2017,**[18]
SiO_2 nanoparticle /hydrophobic GO	VMD at 60 °C	3.5% NaCl	300 Pa vacuum	13.59 LMH	99.99	*J. Memb. Sci.* **2020,**[19]
rGO/PB	**VMD at 20 °C**	**3.5% NaCl**	**0.1 bar vacuum**	**16.1 LMH**	**99.9**	***This Work***
rGO/PB	**VMD at 60 °C**	**3.5% NaCl**	**0.1 bar vacuum**	**167.2 LHM**	**99.9**	***This Work***

Note: The flux values which were approximately obtained from the reported figures were marked with '~' before the values.

References

1 L. Z. Bai, D. L. Zhao, Y. Xu, J. M. Zhang, Y. L. Gao, L. Y. Zhao and J. T. Tang, *Mater. Lett.*, 2012, **68**, 399–401.

2 R. Larciprete, S. Fabris, T. Sun, P. Lacovig, A. Baraldi and S. Lizzit, *J. Am. Chem. Soc.*, 2011, **133**, 17315–17321.

3 H. Yang, L. Sun, J. Zhai, H. Li, Y. Zhao and H. Yu, *J. Mater. Chem. A*, 2014, **2**, 326–332.

4 J. Ederer, P. Janoš, P. Ecorchard, J. Tolasz, V. Štengl, H. Beneš, M. Perchacz and O. Pop-Georgievski, *RSC Adv.*, 2017, **7**, 12464–12473.

5 C. Aparicio, J. Filip and L. Machala, *Powder Diffr.*, 2017, **32**, S207–S212.

6 K. J. Lu, J. Zuo, J. Chang, H. N. Kuan and T. S. Chung, *Environ. Sci. Technol.*, 2018, **52**, 4472–4480.

7 M. Pagliero, A. Bottino, A. Comite and C. Costa, *J. Memb. Sci.*, 2020, **596**, 117575.

8 W. Chen, S. Chen, T. Liang, Q. Zhang, Z. Fan, H. Yin, K. W. Huang, X. Zhang, Z. Lai and P. Sheng, *Nat. Nanotechnol.*, 2018, **13**, 345–350.

9 G. Liu, J. Shen, Q. Liu, G. Liu, J. Xiong, J. Yang and W. Jin, *J. Memb. Sci.*, 2018, **548**, 548–558.

10 Y. Song, R. Li, F. Pan, Z. He, H. Yang, Y. Li, L. Yang, M. Wang, H. Wang and Z. Jiang, *J. Mater. Chem. A*, 2019, **7**, 18642–18652.

11 Y. L. Xue, J. Huang, C. H. Lau, B. Cao and P. Li, *Nat. Commun.*, 2020, **11**, 1461.

12 R. Han and P. Wu, *J. Mater. Chem. A*, 2019, **7**, 6475–6481.

13 Y. Liu, Z. Yu, Y. Peng, L. Shao, X. Li and H. Zeng, *Chem. Phys. Lett.*, 2020, **749**, 137424.

14 E. Yang, A. B. Alayande, C. M. Kim, J. ho Song and I. S. Kim, *Desalination*, 2018, **426**, 21–31.

15 P. Zhang, J. L. Gong, G. M. Zeng, B. Song, H. Y. Liu, S. Y. Huan and J. Li, *Chemosphere*, 2018, **204**, 378–389.

16 J. Zhu, J. Wang, A. A. Uliana, M. Tian, Y. Zhang, Y. Zhang, A. Volodin, K. Simoens, S. Yuan, J. Li, J. Lin, K. Bernaerts and B. Van Der Bruggen, *ACS Appl. Mater. Interfaces*, 2017, **9**, 28990–29001.

17 Y. Han, Y. Jiang and C. Gao, *ACS Appl. Mater. Interfaces*, 2015, **7**, 8147–8155.

18 L. Zhu, H. Wang, J. Bai, J. Liu and Y. Zhang, *Desalination*, 2017, **420**, 145–157.

19 Y. Mao, Q. Huang, B. Meng, K. Zhou, G. Liu, A. Gugliuzza, E. Drioli and W. Jin, *J.*

Memb. Sci., 2020, **611**, 118364.